DELIVERABLE 5.2

Synthesis of operational solutions envisaged for reducing aviation emissions

ACACIA

Advancing the S**c**ience for **A**viation and **Cli**m**a**te

Project Grant Number: 875036
Instrument: Research and Innovation Action (RIA)
Primary Project Coordinator: Dr. Sigrun MATTHES (DLR)
Project Officer: Leonidas SIOZOS-ROUSOULIS
Classification: PU (Public)
Date of Report: June 30, 2022

Responsible partner:
Delft University of Technology (TUD)

European Commission

Authors and contributors to the report

Authors

Name	Role	Institution
Jin Maruhashi	WP contributor	TUD
Prof. Dr. Volker Grewe	WP contributor	TUD/DLR
Dr. Irene Dedoussi	WP5 co-leader	TUD

Contributors

Name	Role	Institution
Dr. Johannes Hendricks	WP contributor	DLR
Dr. Mattia Righi	WP1 co-leader	DLR

Table of Contents

Summary

Aviation's contribution to anthropogenic global warming is estimated to be within the range of 3.5 – 5%, which contemplates both CO_2 and non-CO_2 effects. This range, however, does not consider the contribution from aerosol interactions with liquid clouds (indirect effects) given their high degree of uncertainty. It is thought that such effects are of opposite sign (cooling) and are as large in magnitude as the warming from persistent contrails. Therefore, a more accurate and complete assessment is only possible if aerosol effects are considered. Earlier work has shown that sulphate (SO_4) has a stronger potential to alter lower-level liquid clouds than soot. Therefore, in the context of the ACACIA project, in order to improve our understanding of SO_4 as an indirect climate forcer, we plan to extend the current Lagrangian modelling scheme that has already been successfully applied to the study of gas-phase emissions by developing a tagging approach for aerosols. This would enable us to understand how and where aviation-induced SO_4 interacts with liquid clouds. The first steps required for this modelling transition are outlined in this report. In the near future, once the Lagrangian aerosol scheme is verified and ready, climate change functions that contemplate aerosol-cloud interactions may be produced for the first time. Such an advancement would improve climate-friendly aircraft routing by providing a more complete and therefore accurate mitigation policy.

ACACIA EU Project

This project is funded by the European Union (EU) under the Grant Agreement No. 875036. It began in January 2020 and is part of the Horizon 2020 Research and Innovation Action coordinated by the DLR – Institute of Atmospheric Physics. A total of 11 partner institutions from 7 European countries are involved.

Objective

The purpose of deliverable 5.2 is to describe a course of action to be taken so that the knowledge gained from aerosol-cloud interaction research from previous work packages can be translated to sound strategic advice for greener aircraft operations. Briefly, the main idea is to extend a Lagrangian sub-model (AIRTRAC) that is currently being used within the ECHAM5/MESSy Atmospheric Chemistry (EMAC) global modelling framework to analyze gas-phase emissions so that it will also be capable of following the evolution of aerosol particle mass and number mixing ratios from as early as their introduction into the atmosphere to the point at which they interact with lower-level liquid clouds. Once this model extension is set up and validated, its output may be used to identify climate-sensitive regions with respect to the aerosol indirect effects. This improved understanding will then serve to expand the climate change functions (CCFs) that can be used to further guide climate impact mitigation strategies. In summary, the current report will outline the necessary steps to be taken to adapt the sub-model referred earlier so that it also tracks the evolution of aerosol mass and number mixing ratios along several Lagrangian air parcel trajectories.

This report is divided into two sections: the first is a state-of-the-art on CCFs as well as aerosol climate impacts and the second is a detailed plan on how to adapt the AIRTRAC Lagrangian sub-model so that its output may contribute to the formulation of aerosol-cloud interaction CCFs. This sub-model will be used as a steppingstone in eventually addressing the following key questions:

1. What are the main pathways that are associated with an increase in cloud-forming aerosols from aviation?
2. How do the aerosol mass and number mixing ratios evolve along different trajectories from their emission at a typical subsonic cruise altitude (8-12 km) to the point at which they interact with liquid clouds?
3. Where are lower-level liquid clouds being perturbed by aviation aerosols?

1 State-of-the-art on Aerosol Climate Impacts and CCFs

This first section gauges the current level of understanding of aerosol direct and indirect effects as well as the climate change functions in general. The main knowledge gaps regarding these two topics are then highlighted. The usefulness of algorithmic CCFs (aCCFs) is also briefly discussed.

1.1 Aerosols and their climate impact

Aerosols are airborne particles like sea salt, mineral dust, black carbon (BC) and sulphate (SO_4) that bear a large degree of uncertainty in terms of their climate forcing impact. Aerosols may interfere with Earth's radiative budget by either directly influencing the planetary albedo through its scattering and absorption of shortwave radiation or indirectly by altering the radiative properties of existing clouds, particularly of lower-level liquid clouds (Petzold and Karcher, 2012). Currently, there is a low level

of scientific understanding (LOSU) of direct aerosol effects for either BC or SO_4, as is shown in Figure 1. Results indicate that the former leads to a small overall warming of the atmosphere given that soot absorbs both shortwave solar and outgoing planetary longwave radiations. SO_4 mainly reflects shortwave solar energy, which leads to a cooling effect (Lee et al., 2021; Gettelman and Chen, 2013). In terms of aerosol indirect effects, there is an even lower level of knowledge.

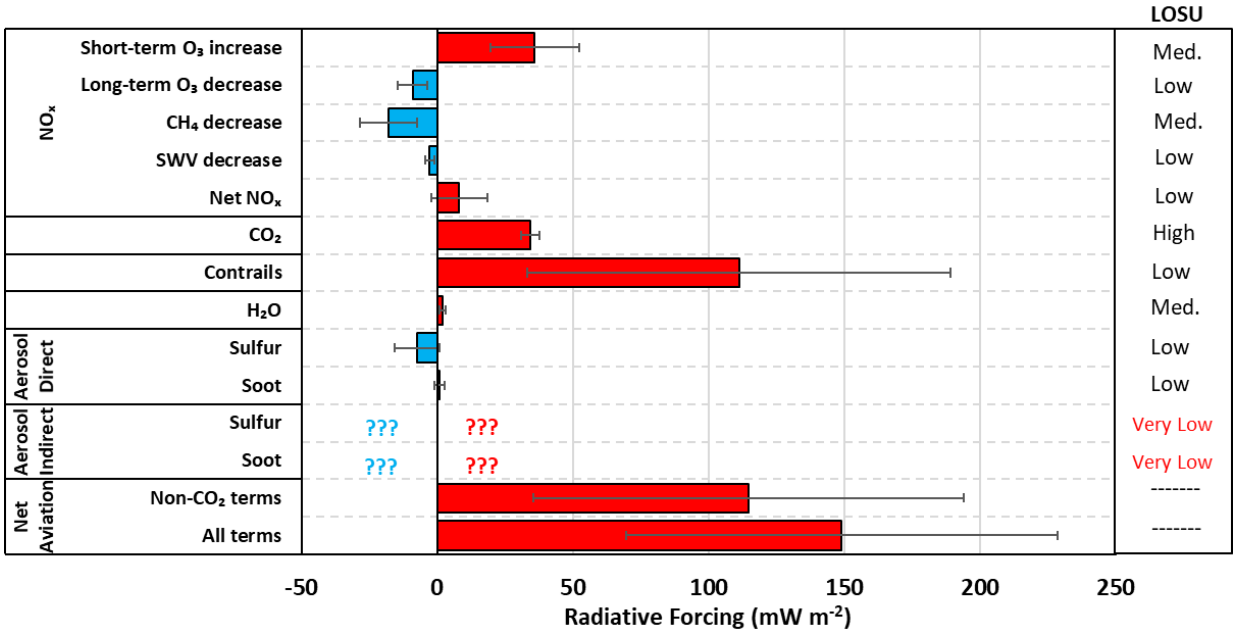

Figure 1 – Overview of aviation climate forcers for the years 1940 – 2018 and their corresponding levels of scientific understanding (LOSU), adapted from (Lee et al., 2021).

Only a few studies have attempted to quantify these impacts from aerosol-cloud interactions in the context of aviation, there are ultimately large differences across several modelling approaches. Gettelman and Chen (2013) for instance, via the Community Atmosphere Model version 5 (CAM5) estimate the global average radiative forcing (RF) from indirect effects of aviation-induced SO_4 particles with a geometric diameter of 14 nm to be a strong cooling effect of -44 mWm^{-2}. The cooling from direct effects is significantly lower, -3 mWm^{-2}. In terms of BC with a geometric diameter of 38 nm, both direct and indirect effects are much lower in magnitude: 8 and 0 mWm^{-2} respectively. Righi et al. (2013), via an EMAC-MADE3 setup, concluded that aviation's main contribution is to the aerosol number concentration in the northern mid-latitudes and also that perturbations to low clouds are primarily responsible for the large cooling effect from aviation in the range of -69.5 – 2.4 mW m^{-2}, depending on the assumptions of the size distributions of emitted particles and on the fuel sulphur content. A companion study (Righi et al., 2016) similarly states that their total RF estimate for aviation is mostly driven by cloud effects associated with an increase in aviation SO_4 emissions.

1.2 What are CCFs?

Climate change functions or CCFs are climate metrics that measure the climate change per unit of emission that a certain type of climate forcer has as a function of the emission time, location and altitude. This equates to stating that CCF data are multidimensional sets comprised of five input variables (Grewe et al., 2014; Simorgh et al., 2022):

$CCF(\text{latitude}, \text{longitude}, \text{altitude}, \text{time}, \text{emission type})$.

Typical emission types for which CCFs have been constructed include nitrogen oxides (NO_x), water vapour (H_2O), contrails, methane (CH_4) as well as the combined effects from NO_x that include the short-term increase in ozone (O_3), the destruction of CH_4 and the decrease in primary mode ozone (PMO). This means that CCFs may be expressed in units of K/kg(fuel), K/kg(N), K/kg(NO_2) or K/km flown for the case of contrail cirrus CCFs. CO_2 CCFs, for instance, would be of less interest as they would simply represent a constant value given their spatially independent and long-term effects. These functions naturally require a climate metric and one that has already been applied is the average temperature response across a 20-year time frame (ATR20; see Eq. 1)(Frömming et al., 2021).

$$\text{ATR20} = \frac{1}{20}\int_{t_0}^{t_0+20} dT(t)dt. \qquad (Eq.\,1)$$

Ultimately, the choice of this metric depends on the research question being addressed as the ATR20 is better suited for short-term assessments while a longer time horizon of 100 years is recommended for long-term climate impacts (Grewe et al., 2014; Frömming et al., 2021). Another feature of CCFs is that they can be dependent on the meteorological conditions in which the emission is introduced, meaning that they may either be weather-dependent and therefore describe how a local emission within a specific weather pattern will influence the surroundings or, alternatively, they may be climatological, in which the climate response to a remote future scenario is assessed (Grewe et al., 2017).

1.3 How are CCFs used?

As stated earlier, climate change functions may be used both in the context of tactical and strategic mitigation options. In the former, the weather conditions on a specific day are considered so that a reduction in the climate impact in the short-term is attempted with weather-dependent CCFs. In the latter, climatological CCFs are applied, with the objective of addressing climate-sensitive regions by adopting longer-term solutions like climate-optimized aircraft design or through more efficient air traffic management (ATM) techniques like intermediate stop operations (Grewe et al., 2017). In either case, CCFs act as inputs to a flight route optimization problem whose solution aims at avoiding regions deemed to be sensitive according to the metric that is used. Naturally, this implies that a trajectory may be optimized according to only a specific type of emission like H_2O or to a combination of climate forcer interactions like the net NO_x effect, some of these will produce conflicting recommendations, thereby making this optimization process a non-trivial matter (Frömming et al., 2013). An additional challenge to be considered is the disagreement with fuel or cost-minimizing routing strategies as climate optimization will likely lead to longer paths that avoid climate-sensitive regions, which can only be achieved at the cost of increased fuel consumption and operating costs (Grewe et al., 2017).

The theory behind climate-optimized trajectory constructions via CCFs is therefore straightforward compared to the execution itself, as the idea is to simply avoid regions in which the values of a chosen CCF are large. Figure 2a (Grewe et al., 2017) shows two possible routes connecting New York (JFK) with Frankfurt (FRA). It highlights the different motivations between Trajectory 1 (shortest distance path that seeks to minimize the flight time and distance) and Trajectory 2 (climate-optimized path based on CCF), where it is clear that the latter aims to avoid highly sensitive (red) areas along its path. Climate-optimized

routing not only applies to two-dimensional (2D) considerations as in Figure 2a but may also be three-dimensional (3D) by including altitudinal changes as in Figure 2b (Lührs et al., 2016).

Amidst a present lack of incentive for airlines to pursue a more time-consuming and costly climate-optimized route, Trajectory 1 is usually chosen by default. As such, a trade-off analysis in the form of a Pareto-front is often useful to convince the aviation industry that a small penalty to their operating cost can come with a much larger benefit in terms of reducing the climate footprint.

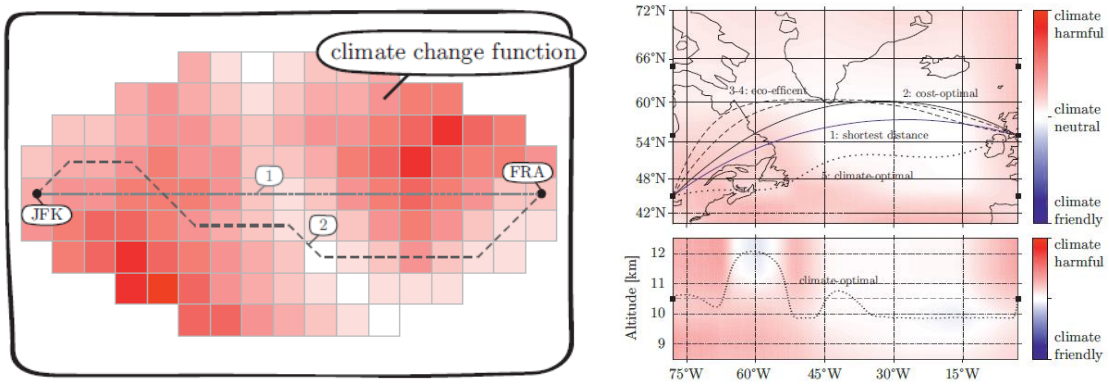

(a) (b)

Figure 2 – (a) Difference between the shortest-distance path (Trajectory 1) and the climate-optimized route (Trajectory 2) for a 2D optimization case (Grewe et al., 2017) and (b) a 3D optimization case with altitudinal changes (Lührs et al., 2016).

From a mathematical standpoint, the Pareto-front (Figure 3) can be generated considering an objective function J that contemplates a cash operating cost (COC) function, the CCF for the forcers mentioned in Eq. 2, the mass flow rate $\dot{m}_i$ of a certain chemical species i, and the v_{TAS} (true airspeed) (Grewe et al., 2017).

$$J = W_{COC} \cdot COC\left(t_{mission}, m_{fuel,mission}\right) \cdot COC_{ref}^{-1} + \cdots$$
$$+W_{CCF} \cdot \left(\sum_{i\epsilon\{CO_2,H_2O,NO_x\}} \int_{t_0}^{t_f} CCF_i(x,t) \cdot \dot{m}_i(t)\, dt + \int_{t_0}^{t_f} CCF_{CiC}(x,t) \cdot v_{TAS}(t) dt \right) \cdot ATR_{20,tot,ref}^{-1} \qquad (Eq.2)$$

The weights W_{COC} and W_{CCF} can vary from 0 to 1 where $W_{CCF} = 0$ would be an entirely cost-minimizing strategy and $W_{COC} + W_{CCF} = 1$. Figure 3 shows the much larger marginal reduction of 15% in the total ATR20 at the cost of only raising the COC by 2% for the 2D case and an even better marginal reduction of 45% for the same 2% cost penalty in the 3D optimization scenario (Grewe et al., 2017). A complete 3D climate-optimized approach is therefore clearly preferred over the 2D alternative.

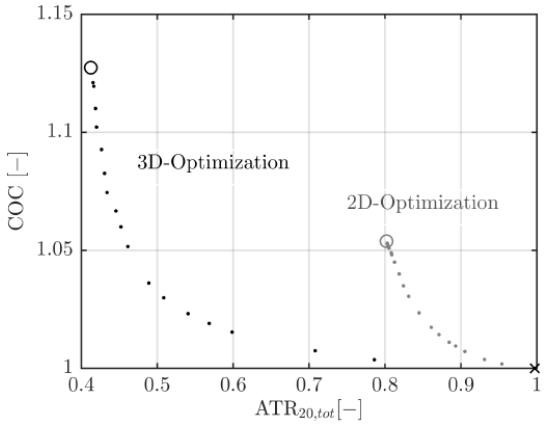

Figure 3 – Pareto-optimal front between Cash Operating Costs and the total climate metric ATR20 for NO_x, H_2O, CO_2 and contrail-induced cirrus effects (Lührs et al., 2016).

1.4 Which CCFs have been developed?

Climate change functions have been developed for CO_2 as well as non-CO_2 climate forcers. The latter typically includes NO_x (including its net effect after CH_4 and PMO decreases), H_2O and contrail cirrus. A recent study by Frömming et al. (2021) has established the weather-dependent CCFs for these non-CO_2 forcers based on a total of 8 representative weather patterns in Summer and in Winter. According to their emission time grid, these CCFs are spatially available for a total of 168 points in space (6 longitudes times 7 latitudes, times 4 pressure levels) along with 3 emission times to reflect the different behaviour of contrails along the time of day. These 168 points, however, mainly cover the North Atlantic flight corridor along with minor areas of North America and Europe (see Figure 4). The NO_x-O_3 CCFs could technically be expanded to a larger, global area if the RF results from Maruhashi et al. (2022) relating to 5 regions (N. America, S. America, Eurasia, Africa and Australasia) were used to update them. The region shown in Figure 4 could then grow to include the main continents.

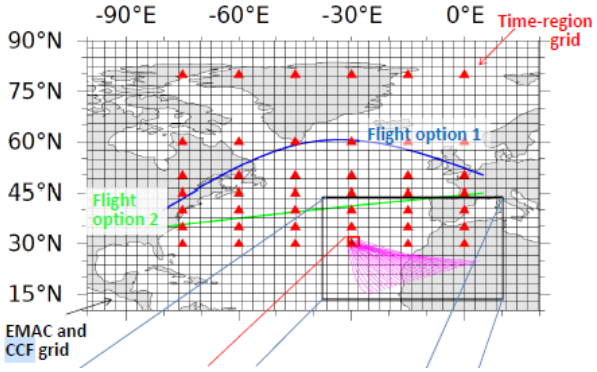

Figure 4 – Time emission grid points for weather-dependent CCFs in the North Atlantic (Grewe et al., 2014).

In the ACACIA project, we will be expanding the existing CCFs efforts towards the eventual inclusion of aerosol-cloud interactions. The development of the sub-model described in Section 2 of this report will therefore be a step in the right direction towards producing these climate change functions.

1.5 Algorithmic CCFs

Algorithmic CCFs or aCCFs were constructed with the objective of reducing the computational burden of calculating the climate impact for a given region with the traditional method of CCFs, since the latter require expensive large-scale simulations from complex climate models. In speeding up and simplifying this process, the possibility of making climate-optimized routing operational becomes more likely. Algorithmic CCFs have been developed for climate impacts arising from NO_x-O_3 chemistry, methane and water vapor emissions by van Manen and Grewe (2019). This was accomplished by applying linear regression techniques to meteorological variables like the geopotential or the temperature of the atmosphere. They found that the potential vorticity was the most relevant parameter for H_2O aCCFs, for O_3 effects the temperature and geopotential were the most important and lastly the CH_4 functions were derived as a function of the geopotential and the incoming solar flux at the top of the atmosphere. The validity of using aCCFs has been addressed, particularly by Rao et al. (2022), in which they investigated how the climate impact would be reduced even if only the NO_x-O_3 aCCFs are considered. They found, despite certain discrepancies during the summer day, that such a method of climate-routing already shows promising results overall.

2 A novel Lagrangian sub-model for aerosol-cloud interaction

This second section describes the necessary steps that would need to be implemented to extend the current AIRTRAC sub-model so that it is able to track how aviation SO_4 emissions contribute to the total SO_4 mass mixing ratio across the 9 aerosol modes available in MADE3: 3 sizes (Aitken (k), accumulation (a) and coarse (c)) × 3 mixing states (Soluble (s), insoluble (i) and mixed (m)). Although the current report focuses only on mass mixing ratios, the same method is applicable to the governing differential equations for SO_4 particle number mixing ratios. As there is currently no tagging available for SO_4 (only for BC) within the context of EMAC, the only way to study the impact of aviation SO_4 on, for instance, the overall SO_4 mass mixing ratio in the atmosphere would be to apply the perturbation approach, which has its limitations (Grewe et al., 2019).

2.1 AIRTRAC and its suitability to the study of transport patterns and chemistry

The AIRTRAC sub-model is currently capable of accompanying the chemical evolution of NO_x, O_3, HNO_3, OH, HO_2, H_2O and CH_4 tracers from a Lagrangian perspective as a result of localized emissions of NO_x and/or H_2O (see supplement of Grewe et al. (2014)). The chemistry calculations are formulated according to the tagging methodology outlined by Grewe (2013) in which a generalized approach for tracking an emission species from an origin based on a sensitivity analysis of the relevant forcing terms from a governing differential equation is described. This tagging equation is shown in Eq. 3:

$$\frac{\partial}{\partial t} x_i^j = P_i^j(t) + F_i(\boldsymbol{x}) \frac{\boldsymbol{x}^{j^T} \nabla F_i(\boldsymbol{x})}{\boldsymbol{x}^T \cdot \nabla F_i(\boldsymbol{x})} \qquad (Eq. 3)$$

where index i denotes the number of state variables x, j is the index for the sources that contribute to a given term, $P_i^j(t)$ is the contribution of source j to the external forcing P_i and F_i is a state-dependent forcing associated with the ith state variable. The time variable is represented by t.

The AIRTRAC sub-model has been applied in a recent study by Maruhashi et al. (2022) in which the main NO_x transport patterns were identified for global emissions released at a typical cruise altitude of 250 hPa

across 5 regions (North America, South America, Eurasia, Africa and Australasia) during 2 representative periods, one during the first day of January 2014 and the other during the first day of July 2014. The short-term increase in O_3 from NO_x emissions was studied and the ensuing radiative forcing effects were quantified. Such effects have been mapped for the complete trajectories of all NO_x emissions, from the point of their release, along their intermediate paths all the way to their final region of impact. A clustering algorithm from neuroscience was applied in this study to systematically help identify the most probable transport paths. This work has therefore set up an approach that will be applied to investigate the transport of SO_4 aerosols and how their microphysical processes evolve along Lagrangian paths once the AIRTRAC sub-model is extended.

2.2 The aerosol equation for the mass mixing ratio

The evolution of the mass mixing ratio $C_{i,m}$ of a given species i and mode m can be expressed most generically with the following governing equation (Aquila et al., 2011):

$$\frac{\partial C_{i,m}}{\partial t} = R(C_{i,m}) + \left.\frac{\partial C_{i,m}}{\partial t}\right|_{g/p} + \left.\frac{\partial C_{i,m}}{\partial t}\right|_{cond} + \left.\frac{\partial C_{i,m}}{\partial t}\right|_{nucl} + \left.\frac{\partial C_{i,m}}{\partial t}\right|_{coag} + \left.\frac{\partial C_{i,m}}{\partial t}\right|_{growth} + \left.\frac{\partial C_{i,m}}{\partial t}\right|_{aging} \quad (Eq.\,4)$$

The meaning of each of the terms listed in Eq. 4 is described in Table 1 below.

Table 1 – definition of the various terms in the generic mass mixing ratio aerosol equation.

Term	Description (Aquila et al., 2011)
$R(C_{i,m})$	Δ in mass mixing ratio of species i in mode m due to transport, emissions, removal processes (dry and wet depositions) and chemistry.
$\left.\frac{\partial C_{i,m}}{\partial t}\right\|_{g/p}$	Δ in mass mixing ratios of NO_3, NH_4 and H_2O from the mass exchange of the partition of HNO_3 and NH_3 into gas and particle phases and the uptake of liquid water.
$\left.\frac{\partial C_{i,m}}{\partial t}\right\|_{cond}$	Refers to the condensation of sulphuric acid (H_2SO_4) and organic vapor on pre-existing particles such that there is mass gained for SO_4 and POM.
$\left.\frac{\partial C_{i,m}}{\partial t}\right\|_{nucl}$	Refers to nucleation of new particles from available H_2SO_4 that has not been consumed by condensation and water contributes to the Aitken soluble mode.
$\left.\frac{\partial C_{i,m}}{\partial t}\right\|_{coag}$	Refers to coagulation or the process of forming larger particles from the collision and sticking of smaller ones. Intermodal coagulation creates particles that are assigned to larger coagulating modes.
$\left.\frac{\partial C_{i,m}}{\partial t}\right\|_{growth}$	Refers to microphysical processes that cause changes in the median diameter of modes. Aitken mode particles may grow and transition to the accumulation mode.
$\left.\frac{\partial C_{i,m}}{\partial t}\right\|_{aging}$	Refers to the aging of, for instance, black carbon and dust particles where insoluble modes are transformed to mixed modes. Pure soluble modes are unaffected by this process.

As has been stated earlier, aviation soot is not considered to pose significant effects on lower-level liquid clouds when compared to SO_4. As a result, the focus will be on the latter aerosol and the modelling

approach will be developed only for this case. Equation 4 may therefore be rewritten for the specific case in which $i = SO_4$. There are then 3 simplifications that may be applied to Eq. 4:

1. There is no gas-to-particle partitioning for SO_4 since it is assumed that H_2SO_4 has a low enough equilibrium vapour pressure such that it is transferred from the gas to the aerosol phase in each time step, but not in the opposite direction (Kaiser et al., 2014).
2. The nucleation term will only affect the soluble Aitken mode (ks) since once SO_4 is formed via this process it is assigned only to this mode.
3. The process of aging will only affect the insoluble and mixed modes, meaning that the soluble (s) modes for any of the 3 sizes (Aitken, accumulation and coarse) are all unaffected.

Applying these assumptions to Eq.4 will lead to the complete set of differential equations describing the evolution of the mass mixing ratio for SO_4 (see Eq. 5):

$$\begin{cases} \frac{\partial C_{SO_4,m}}{\partial t} = R\left(C_{SO_4,m}\right) + \left.\frac{\partial C_{SO_4,m}}{\partial t}\right|_{cond} + \left.\frac{\partial C_{SO_4,m}}{\partial t}\right|_{nucl} + \left.\frac{\partial C_{SO_4,m}}{\partial t}\right|_{coag} + \left.\frac{\partial C_{SO_4,m}}{\partial t}\right|_{growth} ; m \equiv ks \\ \frac{\partial C_{SO_4,m}}{\partial t} = R\left(C_{SO_4,m}\right) + \left.\frac{\partial C_{SO_4,m}}{\partial t}\right|_{cond} + \left.\frac{\partial C_{SO_4,m}}{\partial t}\right|_{coag} + \left.\frac{\partial C_{SO_4,m}}{\partial t}\right|_{growth} + \left.\frac{\partial C_{SO_4,m}}{\partial t}\right|_{aging} ; m \equiv ki, km, ai, am, ci, cs \\ \frac{\partial C_{SO_4,m}}{\partial t} = R\left(C_{SO_4,m}\right) + \left.\frac{\partial C_{SO_4,m}}{\partial t}\right|_{cond} + \left.\frac{\partial C_{SO_4,m}}{\partial t}\right|_{coag} + \left.\frac{\partial C_{SO_4,m}}{\partial t}\right|_{growth} ; m \equiv as, cs \end{cases} \quad (Eq.5)$$

2.2.1 The transport term

The $R\left(C_{SO_4,m}\right)$ term describes the change in SO_4 mass mixing ratio arising from convective, advective and diffusive effects. It also includes mass changes from the introduction of emissions as well as removal processes like sedimentation and dry and wet depositions. These influences are computed outside of the MADE3 aerosol sub-model, for instance, for sedimentation the SEDI (Kerkweg et al., 2006) sub-model is used while for dry (wet) deposition the DDEP (SCAV) (Kerkweg et al., 2006) sub-model is the most appropriate.

2.2.2 The condensation term

The condensation term, in the context of SO_4, refers to the condensation of H_2SO_4 onto existing particles such that there is a net gain in the mass mixing ratio of SO_4. This gain may be expressed in terms of dimensionless coefficients Ω_m and the condensation of H_2SO_4 in each mode m (Aquila et al., 2011):

$$\left.\frac{\partial C_{SO_4,m}}{\partial t}\right|_{cond} = \Omega_m \cdot \Delta C^{cond} \quad (Eq.6a)$$

The coefficients Ω_m may be written in terms of the third moment[1] growth coefficients of mode i, $G_i^{(k)}$:

$$\Omega_m = \frac{G_i^{(3)}}{\sum_{j=1}^{9} G_j^{(3)}} \quad (Eq.6b)$$

The definition of this growth coefficient depends on a size-independent component Ψ_T as well as on the regime of the gas, which is often identified via the Knudsen number[2] (Kn). A free-molecular (fm) regime

[1] The k^{th} moment of a distribution, M_k, is defined as: $M_k = \int_{-\infty}^{\infty} D^k \, n(\ln D) d(\ln D)$ (Aquila et al., 2011).

[2] $Kn = \lambda / L$, $\lambda \equiv$ mean free path or distance a particle travels until colliding, $L \equiv$ characteristic length.

is said to apply when $Kn > 10$ while a near-continuum (nc) regime applies when $Kn < 1$ (Aquila et al., 2011).

$$G_i^{(3)} = \frac{G_i^{(3)fm} G_i^{(3)nc}}{G_i^{(3)fm} + G_i^{(3)nc}};\ G_i^{(3)} = \begin{cases} G_i^{(3)fm} = \frac{6}{\pi}\Psi_T \frac{\pi\alpha\bar{c}}{4}\int_0^\infty D^2 n_i(D)dD\,;\ \ Kn > 10 \\ G_i^{(3)nc} = \frac{6}{\pi}\Psi_T 2\pi D_{\mathrm{v}}\int_0^\infty D n_i(D)dD\,;\ \ Kn < 1 \end{cases} \qquad (Eq.6c)$$

With regard to the expression of the growth coefficient for the free-molecular regime, the α represents the accommodation coefficient and $\bar{c}$ is the mean molecular velocity, which are both treated as constants and independent of a mode's diameter D. The particle number distribution of mode i as a function of its particle diameter is represented by $n_i(D)$. D_{v} in the near-continuum regime is the diffusion constant. In both cases, the component Ψ_T is expressed according to Eq. 6d in terms of the molecular weight $M_{\mathrm{H_2SO_4}}$, the density ρ and the saturation ratio S_{v} of the condensing gas, as well as the saturation vapor pressure for H_2SO_4, p_{s,H_2SO_4}, the universal gas constant R and the temperature T:

$$\Psi_T = \frac{M_{\mathrm{H_2SO_4}} \cdot p_{\mathrm{s,H_2SO_4}} \cdot (S_{\mathrm{v}} - 1)}{\rho R T}. \qquad (Eq.6d)$$

The term ΔC^{cond} represents the H_2SO_4 mass mixing ratio arising solely due to condensation, which is obtained by subtracting the production contribution term $P\Delta t$ from the change in the analytical solution (Eq.7b) to the ordinary differential equation (ODE) in Eq.7a that describes the evolution of the mass mixing ratio of gas-phase H_2SO_4 (neglecting a nucleation term):

$$\frac{dC_{H_2SO_4}(t)}{dt} = P - L \cdot C_{H_2SO_4}(t). \qquad (Eq.7a)$$

$$C_{H_2SO_4}(t) = \frac{P}{L} + \left(C_{H_2SO_4}(t_0) - \frac{P}{L}\right) e^{-L(t-t_0)} \qquad (Eq.7b)$$

The change in the mass mixing ratio of H_2SO_4 ($\Delta C_{H_2SO_4}$) since the initial time step t_0 is then simply the difference between Eq. 7b and the initial mixing ratio $C_{H_2SO_4}(t_0)$:

$$\Delta C_{H_2SO_4}(t_0) = \frac{P}{L} + \left(C_{H_2SO_4}(t_0) - \frac{P}{L}\right) e^{-L(t-t_0)} - C_{H_2SO_4}(t_0) = \left(\frac{P}{L} - C_{H_2SO_4}(t_0)\right)\left(1 - e^{-L(t-t_0)}\right).$$

The ΔC^{cond} is the difference between $\Delta C_{H_2SO_4}(t_0)$ and $P\Delta t$:

$$\Delta C^{cond} = \left(\frac{P}{L} - C_{H_2SO_4}(t_0)\right)\left(1 - e^{-L(t-t_0)}\right) - P\Delta t \qquad (Eq.8)$$

Lastly, the loss term L in Eq.8 is calculated by assuming that the loss of gas-phase H_2SO_4 becomes the gain of SO_4 across all 9 modes (Aquila et al., 2011):

$$L = \sum_{i=1}^{9} \frac{\partial C_{SO_4,i}}{\partial t} = \rho_{SO_4} \frac{\pi}{6} \sum_{i=1}^{9} G_i^{(3)} \qquad (Eq.9)$$

where ρ_{SO_4} is the specific density of SO_4 and L can then be calculated by applying Eq.6c to Eq.9.

2.2.3 The nucleation term

Sulfate aerosols form in the atmosphere primarily from the homogenous nucleation of sulfuric acid and water. Nucleation is therefore a critical process that must be considered in the study of SO_4 and is often parameterized, especially in large-scale models, in order to reduce the overall computational cost (Vehkamäki et al., 2002). MADE3 applies the parameterization for the binary H_2SO_4-H_2O homogeneous nucleation rate J developed by Vehkamäki et al. (2002) that is valid for the troposphere and stratosphere for a temperature range between 230.15 – 300.15 K, a relative humidity range between 0.01 – 100% and an H_2SO_4 mixing ratio in the range 10^4 – 10^{11} cm^{-3}. It is assumed that the newly nucleated sulfate particles are composed entirely of a representative diameter[3] of 3.5 nm, even though in reality they are likely to be smaller and grow to more comparable sizes via other processes like coagulation and condensation, as is acknowledged by Binkowski and Roselle (2003). The calculation of the nucleation term is then performed according to Eq.10 (Aquila et al., 2011):

$$\left.\frac{\partial C_{SO_4,ks}}{\partial t}\right|_{nucl} = J\left(T, RH, C_{H_2SO_4}\right) \times m_{3.5nm}(RH) \times \exp\left[\frac{9}{2}\ln^2 \sigma_{ks}\right] \qquad (Eq.10)$$

where J is the parameterized nucleation rate from (Vehkamäki et al., 2002) that depends on atmospheric conditions like the temperature T and the relative humidity RH as well as on the mixing ratio of H_2SO_4: $C_{H_2SO_4}$. The term $m_{3.5nm}(RH)$ denotes the mass of SO_4 present within a particle with a wet diameter of 3.5 nm while the $\exp\left[\frac{9}{2}\ln^2 \sigma_{ks}\right]$ term contains the geometric standard deviation of the soluble Aitken mode, both of which reflect the assumption that freshly nucleated particles with the given diameter are attributed entirely to this mode. It is worth noting, however, that nucleation involves only the amount of H_2SO_4 that has not yet been consumed via condensation according to Eq. 7a (Aquila et al., 2011). This means that there is a competition between these two processes and that nucleation only occurs in regions where condensational sinks for H_2SO_4 are low.

2.2.4 The coagulation term

Two types of coagulation processes are distinguished: intra and intermodal. The former occurs between the same mode and produces particles that belong in the same class as the original ones. The latter occurs between particles of different modes and produces particles that are part of the larger of the two colliding classes. Only intermodal coagulation is of interest in the current case as intramodal coagulation is mass-conserving relative to its class. The coagulation contribution to mode k of colliding particles belonging to modes l and m is given by the following relation (Kaiser et al., 2014):

[3] In Kaiser et al. (2019) and subsequent studies, a value of 10 nm is used to account for the newly nucleated particles growing quickly and reaching larger sizes within hours. Seeing as the global model cannot resolve this fast particle growth, a larger diameter is normally assumed immediately after formation.

$$\left.\frac{\partial C_{SO_4,k}}{\partial t}\right|_{coag} = \frac{\pi}{6}\sum_{l=1}^{9}\sum_{m=1}^{9}[(\delta_{k,\tau_{lm}} - \delta_{k,l}) \cdot \frac{C_{SO_4,l}}{\sum_{s=1}^{A} C_{s,l}} \cdot \rho_l \int_0^{\infty}\int_0^{\infty} (D_1)^3 \beta(D_1, D_2) n_l(D_1) n_m(D_2) dD_1 dD_2 + \ldots$$
$$\ldots + (\delta_{k,\tau_{lm}} - \delta_{k,m}) \cdot \frac{C_{SO_4,m}}{\sum_{s=1}^{A} C_{s,m}} \cdot \rho_m \int_0^{\infty}\int_0^{\infty} (D_2)^3 \beta(D_1, D_2) n_l(D_1) n_m(D_2) dD_1 dD_2] \quad (Eq.\,11)$$

The decision criteria to determine the mode to which a coagulated particle will be added is directly related to the τ_{lm} term and is summarized in Table 2 (Kaiser et al., 2014). Given the complexity of Eq. 11, each variable is defined separately in Table 3.

Table 2 – Values of τ_{lm} based on origin modes l (rows) and m (columns), which are numbered as follows: ks=1, km=2, ki=3, as=4, am=5, ai=6, cs=7, cm=8 and ci=9. Table 2 was adapted from (Kaiser et al., 2014).

Modes	ks	km	ki	as	am	ai	cs	cm	ci
ks	1	2	2/3*	4	5	5/6*	7	8	9
km	2	2	2/3*	5	5	5/6*	8	8	9
ki	2/3*	2/3*	3	3/5*	3/5*	6	8	8	9
as	4	5	3/5*	4	5	5/6*	7	8	8/9*
am	5	5	3/5*	5	5	5/6*	8	8	8/9*
ai	5/6*	5/6*	6	5/6*	5/6*	6	6/8*	6/8*	9
cs	7	8	8	7	8	6/8*	7	8	8/9*
cm	8	8	8	8	8	6/8*	8	8	8/9*
ci	9	9	9	8/9*	8/9*	9	8/9*	8/9*	9

The * denotes a case in which the coagulated particle is placed in one of two modes depending on its soluble mass fraction x relative to water. If $x = 1$ then the resulting particle is placed in the soluble mode, if $x\epsilon[0.1,1[$ it is placed in the mixed mode and if $x\epsilon[0,0.1[$ it is placed in the insoluble mode (Aquila et al., 2011; Kaiser et al., 2014).

2.2.5 The growth term

Aerosol particles may grow as they coagulate or as they condense onto other particles. In such cases, particles may be redistributed to a larger size class, i.e., from Aitken to accumulation mode. This is important to then ensure consistency in their size distribution across the different modes. In MADE3, particle growth is handled through a procedure called renaming wherein one of the following two conditions must be fulfilled (Kaiser et al., 2014):

1. The volume growth rate (growth of third moment $G^{(3)}$) of the Aitken mode is larger than the volume growth rate of the accumulation mode and its number mixing ratio is also larger.
2. Median diameter of the Aitken mode is larger than 30 nm and its number mixing ratio is larger than the number mixing ratio in the accumulation mode.

When at least one of the above conditions is met, the number mixing ratio of the particles larger than an intersection diameter D_N (see Eq.12 (Aquila et al., 2011)) between the two number size distributions (Aitken and accumulation) is then renamed from Aitken to accumulation mode. The same applies to the corresponding mass mixing ratio. This renaming process is only performed between Aitken and accumulation modes for particles of the same mixing state, i.e., ks and as, ki and ai or km and am (Aquila et al., 2011; Kaiser et al., 2014). The number of particles from the Aitken mode that will be renamed in

this mode is given by Eq. 12, where "erf" is the error function, N_t is the total particle number mixing ratio of the mode, D_g is the median diameter of the mode and σ_g is the width or the geometric standard deviation of the mode:

$$N(D_N) = \frac{N_t}{2}\left[1 + \mathrm{erf}\left(\frac{\ln(D_N/D_g)}{\sqrt{2}\ln\sigma_g}\right)\right]. \qquad (Eq.\,12)$$

2.2.6 The aging term

The aerosol aging process refers to the transformation of insoluble particles via the acquisition of a soluble coating that modifies their state from hydrophobic to hydrophilic (Kaiser et al., 2014), it will therefore only impact the insoluble and mixed modes of SO_4. Aquila et al. (2011) highlight two scenarios that are of relevance to aging. The first describes the situation in which the entire mass and number mixing ratios of an externally mixed mode is redistributed across the Aitken and accumulation modes with BC and dust as a result of their aging from, for instance, the condensation of SO_4, coagulation or even the uptake of H_2O, NH_4 or NO_3. Two decisions must be made regarding this process:

1. The event of redistributing the externally mixed mode across the km and am modes will occur if the soluble mass fraction of SO_4 is larger than 10%.
2. Once the first condition is met, the intersection diameter D_N (see Eq. 12) will be used to decide how much of the externally mixed mode will be distributed to mode km and am. The externally mixed particles with sizes smaller than D_N will be allocated to km and those larger than D_N are placed in the am mode.

The second scenario in which aging can occur is when externally mixed BC particles that are taken up by cloud droplets but not rained out are considered to be aged after the evaporation of the cloud and allocated to the internally mixed mode. Further details are available in (Aquila et al., 2011).

2.3 Application of the tagging approach to the aerosol mass mixing ratio equation

In order to quantify the contribution from aviation to the overall SO_4 mass mixing ratio, two sets of differential equations must be considered, for a total of 18 equations. The first one is for the background (b) contribution and the second is naturally for aviation emissions (e). This means that for each of these sources, a set of equations like the ones found in Eq. 5 will be produced. The total contribution to the SO_4 mass mixing ratio will therefore be the sum of both parcels (see Eq. 13):

$$\frac{\partial C_{SO_4}}{\partial t} = \left.\frac{\partial C_{SO_4}}{\partial t}\right|_b + \left.\frac{\partial C_{SO_4}}{\partial t}\right|_e \qquad (Eq.\,13)$$

Referring back to the tagging approach presented in Section 2.1, this equates to stating that there is a total of nine state variables corresponding to the SO_4 mass mixing ratios that result from the nine aerosol modes in MADE3 ($C_{SO_4,ks}, C_{SO_4,km}, C_{SO_4,ki}, \ldots, C_{SO_4,ci}$) with two sources (background and aviation emissions). In order to illustrate the application of this method, a simplified scenario will be studied in which the different processes (condensation, coagulation, nucleation, …) are considered separately for a single state variable. This is possible given the uncoupled nature of the differential equations of Eq. 5 for each aerosol mode. The tagging approach will be applied to two cases in this report: the nucleation process in the soluble Aitken mode and the coagulation process also in the soluble Aitken mode. This

methodology is also applicable to the governing differential equations for the aerosol particle number mixing ratios (Eq. 6 in Aquila et al. (2011)), but these formulations are not included in this report.

2.3.1 The nucleation process in the soluble Aitken mode for SO_4

The governing differential equation pertaining to the nucleation of SO_4 only applies to the soluble Aitken mode, as is stated in Eq. 10. In the context of the tagging methodology, Eq. 10 only has a forcing term that is time-dependent given that the nucleation rate itself is a function of time-varying atmospheric conditions like the temperature and relative humidity. This leads to the simplification of Eq. 3 in the following manner:

$$\frac{\partial}{\partial t} x_i^j = P_i^j(t) \qquad (Eq.\,14)$$

Since there are 2 sources (background and aviation emissions) and 1 state variable ($C_{SO_4,ks}$) involved, the tagging approach yields Eqs. 15a and b for the background and aviation emissions contributions respectively:

$$\left.\frac{\partial C_{SO_4,ks}}{\partial t}\right|_{nucl}^{b} = \frac{C_{H_2SO_4}|_b}{C_{H_2SO_4}} \times J\left(T, RH, C_{H_2SO_4}\right) \times m_{3.5nm}(RH) \times \exp\left[\frac{9}{2}\ln^2 \sigma_{ks}\right] \qquad \text{(Eq. 15a)}$$

$$\left.\frac{\partial C_{SO_4,ks}}{\partial t}\right|_{nucl}^{e} = \frac{C_{H_2SO_4}|_e}{C_{H_2SO_4}} \times J\left(T, RH, C_{H_2SO_4}\right) \times m_{3.5nm}(RH) \times \exp\left[\frac{9}{2}\ln^2 \sigma_{ks}\right] \qquad (Eq.\,15b)$$

where the relative weights $\frac{C_{H_2SO_4}|_b}{C_{H_2SO_4}}$ and $\frac{C_{H_2SO_4}|_e}{C_{H_2SO_4}}$ denote the H_2SO_4 mass mixing ratio fractional contributions from background and aviation, respectively. The sum of Eqs. 15a and b will then yield the total effect from nucleation to the soluble Aitken mode of SO_4, similarly to what is shown by Eq. 13.

2.3.2 The coagulation process in the soluble Aitken mode for SO_4

The coagulation of SO_4 involves a forcing term that is state-dependent, as can be seen by the fractional mass term preceding the particle density in Eq. 11. The application of the tagging equation (Eq. 3) in this section focuses on the Aitken soluble (ks) mode, so that $k = 1$ in Eq. 11. The first step is to therefore simplify the right-hand side (RHS) of this equation by evaluating the Kronecker deltas, the τ_{lm} term and by expanding the double summation. Table A1 in the Appendix shows all of the coefficients that result from the Kronecker deltas upon expanding the summation. Evidently, not all non-zero terms will contribute to the formulation as only combinations of two distinct modes should be counted. As an example, the coagulation involving the soluble Aitken and the mixed accumulation modes can be found by either setting $l = 1$ and $m = 5$ or $l = 5$ and $m = 1$, however, the term should only be counted once. If the coefficients in Table A1 for these options are used in Eq. 11, the same expression is produced. It is also worth verifying in the same table that all intramodal coagulation scenarios ($l = m$) lead to 0, as is to be expected when considering the mass mixing ratio equation.

For consistency with the variables in Eq. 3 and improved readability, the nine SO_4 modes will be rewritten as follows:

$x_1 = C_{SO_4,ks}, x_2 = C_{SO_4,km}, x_3 = C_{SO_4,ki}, x_4 = C_{SO_4,as}, x_5 = C_{SO_4,am}, x_6 = C_{SO_4,ai}, x_7 = C_{SO_4,cs}, x_8 = C_{SO_4,cm}, x_9 = C_{SO_4,ci}$.

According to Table A1, there are 8 non-zero terms that should be contemplated in the current formulation, these correspond to the following modes: $(l,m) = (1,2),(1,3),(1,4),(1,5),(1,6),(1,7),(1,8),(1,9)$. In all of these cases, $\tau_{lm} \neq k = 1$. This means that all intermodal coagulation events will lead to a negative change in the mass mixing ratio of SO_4, hence the negative sign in Eq.16. In other words, the particles that begin in the ks mode are transferred to another class after colliding with other particles. Including these terms into Eq. 11 yields the following:

$$\frac{\partial}{\partial t}x_1 = -\frac{\rho_1 \pi}{6} \cdot \frac{x_1}{x_1 + C}\left[f_{1,2}(D_1,D_2) + f_{1,3}(D_1,D_2) + f_{1,4}(D_1,D_2) + f_{1,5}(D_1,D_2) + f_{1,6}(D_1,D_2) + f_{1,7}(D_1,D_2) + f_{1,8}(D_1,D_2) + f_{1,9}(D_1,D_2)\right]$$

where the integrals of the Brownian coagulation kernels $\beta(D_1,D_2)$ between modes l and m have been compactly defined as $f_{l,m}(D_1,D_2) = \int_0^\infty \int_0^\infty (D_1)^3 \beta(D_1,D_2) n_l(D_1) n_m(D_2) dD_1 dD_2$ and the C term in the denominator represents the sum of the mass mixing ratios of the other 8 tracers in mode $l = 1$, i.e., $C = C_{NH_4,1} + C_{NO_3,1} + C_{Na,1} + C_{Cl,1} + C_{POM,1} + C_{BC,1} + C_{DU,1} + C_{H_2O,1}$. The sum of coagulation kernels may be treated as a constant in the partial differentiation process as it depends on the diameters of the colliding modes so the equation above may be simplified even further:

$$\frac{\partial}{\partial t}x_1 = -K\frac{x_1}{x_1 + C} \qquad (Eq.16)$$

which is of the form $\frac{\partial}{\partial t}x_1 = F_1(x)$. In order to derive an expression for the contribution of aviation emissions to the rate of change of the mass mixing ratio of SO_4 for the soluble Aitken mode ($\frac{\partial}{\partial t}x_1^e$), Eq. 3 is applied to Eq. 16, noting that the time-dependent forcing term is not present.

$$\frac{\partial}{\partial t}x_1^e = F_1(\boldsymbol{x})\frac{\boldsymbol{x}^{j^T}\nabla F_1(\boldsymbol{x})}{\boldsymbol{x}^T \nabla F_i(\boldsymbol{x})} \qquad (Eq.17)$$

Substituting the expression for $F_1(x)$ in Eq. 17 yields:

$$\frac{\partial}{\partial t}x_1^e = F_1(x)\frac{(x_1^e, x_2^e, x_3^e, \dots, x_9^e)\left(\frac{-KC}{(x_1+C)^2}, 0,0, \dots, 0\right)^T}{(x_1, x_2, x_3, \dots, x_9)\left(\frac{-KC}{(x_1+C)^2}, 0,0, \dots, 0\right)^T} = F_1(x)\frac{x_1^e}{x_1}$$

which is the self-dependency case in (Kaiser et al., 2014). Lastly, replacing the term for $F_1(x)$ above and simplifying leads to the tagging equation for aviation emissions in the final form:

$$\frac{\partial}{\partial t}x_1^e = -K\frac{x_1^e}{x_1 + C} \qquad (Eq.18)$$

where the parameter K mainly represents the possible binary aerosol collision outcomes:

$$K = \frac{\rho_1 \pi}{6}\sum_{i=2}^{9} f_{l=1,i}(D_1,D_2).$$

Table 3 – Definition of variables in coagulation equation (Eq.11) for the mass mixing ratio of SO_4.

Variable	Description
Kronecker delta ($\delta_{x,y}$)	$\delta_{x,y} = \begin{cases} 1, x = y \\ 0, x \neq y \end{cases}$
Matrix for mode assignment (τ_{lm})	See Table 2, this matrix is used to determine the mode to which the mass mixing ratio of a coagulated particle will be attributed. Note the following numbering of the 9 modes: ks=1, km=2, ki=3, as=4, am=5, ai=6, cs=7, cm=8 and ci=9.
$C_{SO_4,l}$ or $C_{SO_4,m}$	Mass mixing ratio of SO_4 corresponding to modes l or m.
A from sigma notation	Represents the number of tracer species, for MADE3 this means 9: SO_4, NH_4, NO_3, Na, Cl, POM, BC, DU, H_2O.
ρ_l and ρ_m	Particle densities for mode l and m
D_1 and D_2	Particle diameters
$n_l(D)$ and $n_m(D)$	Number distribution for modes l and m for particles of diameter D
$\beta(D_1, D_2)$	Describes the collision probability between particles of diameters D_1 and D_2 based on Brownian motion. The expressions vary according to the aerosol regime, which is characterized by the Knudsen number Kn. As was done in Eq.6c, each of the two regimes (free-molecular and continuum) will have their own expression (Whitby et al., 1991): $$\beta(D_1, D_2) = \begin{cases} \sqrt{\frac{6k_BT}{\rho_1 + \rho_2}} \cdot \left(\sqrt{D_1} + 2\frac{D_2}{\sqrt{D_1}} + \frac{(D_2)^2}{(D_1)^{\frac{3}{2}}} + \frac{(D_1)^2}{(D_2)^{\frac{3}{2}}} + 2\frac{D_1}{\sqrt{D_2}} + \sqrt{D_2} \right); Kn > 10 \\ \frac{2k_BT}{3v} \cdot \left[2 + 2\lambda A \left(\frac{1}{D_1} + \frac{D_2}{(D_1)^2} \right) + 2\lambda A \left(\frac{1}{D_2} + \frac{D_1}{(D_2)^2} \right) + \frac{D_2}{D_1} + \frac{D_1}{D_2} \right]; Kn < 1 \end{cases}$$ where k_B is Boltzmann's constant, v is the atmospheric dynamic viscosity given by $B \cdot \frac{T^{3/2}}{T+S}$ and $\lambda = \Lambda \cdot \frac{p_0 T}{T_0 p}$. The relevant constants are: $A = 1.246$, $B = 1.458 \times 10^{-6}$kgm^{-1}s^{-1}K$^{-0.5}$, $S = 110.4$K, $\Lambda = 6.6328 \times 10^{-8}$m, $p_0 = 101.325$hPa and $T_0 = 288.15$K.

Conclusions

The objective of the current report is to describe a course of action that is to be implemented in order to extend the Lagrangian sub-model AIRTRAC so that it may also apply to the study of aerosols, more specifically to SO_4. Once this is accomplished, the natural next step would be to compare the results obtained with other modelling approaches and once validated, to translate them into climate change functions that may help identify greener flight trajectories. In describing this process, a summary of CCFs has also been provided.

Currently, the non-CO_2 effects that climate change functions can contemplate are limited to H_2O and NO_x emissions as well as persistent contrails. Significant advances have been made to characterize the indirect climate effects from NO_x emissions concerning their induced short-term increase in O_3, longer-term decrease in CH_4 and lastly the reduction in background O_3 or PMO that arises from the decrease in CH_4 all as a function of emission location and time as well as of the meteorological conditions like temperature or geopotential height. The main secondary effect that has not yet been included thus far is the decrease in stratospheric water vapour resulting from less CH_4 entering the stratosphere and decomposing into CO_2 and H_2O. The main knowledge gap that exists with CCFs, however, relates to aerosols, including both direct and indirect effects. For aviation, the more relevant aerosol type to focus on would be SO_4 given its stronger potential to alter the microphysical properties of clouds when compared to soot. In the future, as more CCFs for different regions and conditions become available, the less computationally intensive aCCFs may then be developed to help operationalize them for daily flight route planning.

The AIRTRAC sub-model was constructed based on a tagging approach that allows for the tracking of the contribution of aviation emissions to the atmosphere. It presently only considers the possible effects from NO_x and H_2O emissions and how these affect the volume mixing ratios of the tracers NO_x, O_3, HNO_3, OH, HO_2, H_2O and CH_4. To extend it to the context of aerosols and therefore provide the first-ever possibility of tagging SO_4 in a Lagrangian manner (at least within the context of EMAC), it is necessary to once again apply the generalized tagging methodology but now to the aerosol dynamics equations describing the rate of change of SO_4 mass mixing ratio across the 9 mixing states. An initial attempt at formulating these tagging equations is made here for two simple cases: nucleation and coagulation processes for the soluble Aitken mode of SO_4.

In conclusion, this deliverable has summarized the main points regarding the current knowledge on CCFs and has also traced an achievable path to extending the modelling infrastructure in use to allow for a more detailed analysis of aerosol-cloud interactions from a Lagrangian perspective.

Appendix

Table A1 – Evaluation of all terms from the coagulation equation (Eq.11) contributing to the change in the mass mixing ratio of the soluble Aitken mode of SO_4. The highlighted rows denote the ambiguous cases (asterisks in Table 2) that can only be determined depending on the soluble mass fraction so both scenarios are considered.

l	m	Tau_lm	delta(k,tau)-delta(k,l)	delta(k,tau)-delta(k,m)
1	1	1	0	0
1	2	2	-1	0
1	3	2	-1	0
1	3	3	-1	0
1	4	4	-1	0
1	5	5	-1	0
1	6	5	-1	0
1	6	6	-1	0
1	7	7	-1	0
1	8	8	-1	0
1	9	9	-1	0
2	1	2	0	-1
2	2	2	0	0
2	3	2	0	0
2	3	3	0	0
2	4	5	0	0
2	5	5	0	0
2	6	5	0	0
2	6	6	0	0
2	7	8	0	0
2	8	8	0	0
2	9	9	0	0
3	1	2	0	-1
3	1	3	0	-1
3	2	2	0	0
3	2	3	0	0
3	3	3	0	0
3	4	3	0	0
3	4	5	0	0
3	5	3	0	0
3	5	5	0	0
3	6	6	0	0
3	7	8	0	0
3	8	8	0	0
3	9	9	0	0
4	1	4	0	-1

4	2	5	0	0
4	3	3	0	0
4	3	5	0	0
4	4	4	0	0
4	5	5	0	0
4	6	5	0	0
4	6	6	0	0
4	7	7	0	0
4	8	8	0	0
4	9	8	0	0
4	9	9	0	0
5	1	5	0	-1
5	2	5	0	0
5	3	3	0	0
5	3	5	0	0
5	4	5	0	0
5	5	5	0	0
5	6	5	0	0
5	6	6	0	0
5	7	8	0	0
5	8	8	0	0
5	9	8	0	0
5	9	9	0	0
6	1	5	0	-1
6	1	6	0	-1
6	2	5	0	0
6	2	6	0	0
6	3	6	0	0
6	4	5	0	0
6	4	6	0	0
6	5	5	0	0
6	5	6	0	0
6	6	6	0	0
6	7	6	0	0
6	7	8	0	0
6	8	6	0	0
6	8	8	0	0
6	9	9	0	0
7	1	7	0	-1
7	2	8	0	0
7	3	8	0	0
7	4	7	0	0
7	5	8	0	0
7	6	6	0	0

7	6	8	0	0
7	7	7	0	0
7	8	8	0	0
7	9	8	0	0
7	9	9	0	0
8	1	8	0	-1
8	2	8	0	0
8	3	8	0	0
8	4	8	0	0
8	5	8	0	0
8	6	6	0	0
8	6	8	0	0
8	7	8	0	0
8	8	8	0	0
8	9	8	0	0
8	9	9	0	0
9	1	9	0	-1
9	2	9	0	0
9	3	9	0	0
9	4	8	0	0
9	4	9	0	0
9	5	8	0	0
9	5	9	0	0
9	6	9	0	0
9	7	8	0	0
9	7	9	0	0
9	8	8	0	0
9	8	9	0	0
9	9	9	0	0

References

Aquila, V., Hendricks, J., Lauer, A., Riemer, N., Vogel, H., Baumgardner, D., Minikin, A., Petzold, A., Schwarz, J. P., Spackman, J. R., Weinzierl, B., Righi, M., and Dall'Amico, M.: MADE-in: a new aerosol microphysics submodel for global simulation of insoluble particles and their mixing state, Geosci. Model Dev., 4, 325–355, https://doi.org/10.5194/gmd-4-325-2011, 2011.

Binkowski, F. S. and Roselle, S. J.: Models-3 community multiscale air quality (CMAQ) model aerosol component – 1. Model description, J. Geophys. Res.-Atmos., 108, 4183, doi:10.1029/2001JD001409, 2003.

Frömming, C., Grewe, V., Jöckel, P., Brinkop, S., Dietmüller, S., Garny, H., Ponater, M., Tsati, E. and Matthes, S.: Climate cost functions as a basis for climate optimized flight trajectories. *Tenth USA/Europe Air Traffic Management Research and Development Seminar (ATM2013)*, Chicago, Illinois, 2013.

Frömming, C., Grewe, V., Brinkop, S., Jöckel, P., Haslerud, A. S., Rosanka, S., van Manen, J., and Matthes, S.: Influence of weather situation on non-CO2 aviation climate effects: the REACT4C climate change functions, Atmos. Chem. Phys., 21, 9151–9172, https://doi.org/10.5194/acp-21-9151-2021, 2021.

Gettelman, A. and Chen, C.: The climate impact of aviation aerosols, *Geophys. Res. Lett., 40,* 2785-2789, doi:10.1002/grl.50520, 2013.

Grewe, V.: A generalized tagging method, Geosci. Model Dev., 6, 247–253, https://doi.org/10.5194/gmd-6-247-2013, 2013.

Grewe, V., Frömming, C., Matthes, S., Brinkop, S., Ponater, M., Dietmüller, S., Jöckel, P., Garny, H., Tsati, E., Dahlmann, K., Søvde, O. A., Fuglestvedt, J., Berntsen, T. K., Shine, K. P., Irvine, E. A., Champougny, T., and Hullah, P.: Aircraft routing with minimal climate impact: the REACT4C climate cost function modelling approach (V1.0), Geosci. Model Dev., 7, 175–201, https://doi.org/10.5194/gmd-7-175-2014, 2014.

Grewe, V., Dahlmann, K., Flink, J., Frömming, C., Ghosh, R., Gierens, K., Heller, R., Hendricks, J., Jöckel, P., Kaufmann, S., Kölker, K., Linke, F., Luchkova, T., Lührs, B., Van Manen, J., Matthes, S., Minikin, A., Niklaß, M., Plohr, M., Righi, M., Rosanka, S., Schmitt, A., Schumann, U., Terekhov, I., Unterstrasser, S., Vázquez-Navarro, M., Voigt, C., Wicke, K., Yamashita, H., Zahn, A., Ziereis, H. Mitigating the Climate Impact from Aviation: Achievements and Results of the DLR WeCare Project. Aerospace, 4, 34. https://doi.org/10.3390/aerospace4030034, 2017.

Grewe, V., Matthes, S. and Dahlmann, K.: The contribution of aviation NOx emissions to climate change: are we ignoring methodological flaws?. Environ. Res. Lett. 14 121003, https://doi.org/10.1088/1748-9326/ab5dd7, 2019.

Kaiser, J. C., Hendricks, J., Righi, M., Riemer, N., Zaveri, R. A., Metzger, S., and Aquila, V.: The MESSy aerosol submodel MADE3 (v2.0b): description and a box model test, Geosci. Model Dev., 7, 1137–1157, https://doi.org/10.5194/gmd-7-1137-2014, 2014.

Kaiser, J. C., Hendricks, J., Righi, M., Jöckel, P., Tost, H., Kandler, K., Weinzierl, B., Sauer, D., Heimerl, K., Schwarz, J. P., Perring, A. E., and Popp, T.: Global aerosol modeling with MADE3 (v3.0) in EMAC (based on v2.53): model description and evaluation, Geosci. Model Dev., 12, 541–579, https://doi.org/10.5194/gmd-12-541-2019, 2019.

Kerkweg, A., Buchholz, J., Ganzeveld, L., Pozzer, A., Tost, H., and Jöckel, P.: Technical Note: An implementation of the dry removal processes DRY DEPosition and SEDImentation in the Modular

Earth Submodel System (MESSy), Atmos. Chem. Phys., 6, 4617–4632, https://doi.org/10.5194/acp-6-4617-2006, 2006.

Lee, D.S., Fahey, D.W., Skowron, A., Allen, M.R., Burkhardt, U., Chen, Q., Doherty, S.J., Freeman, S., Forster, P.M., Fuglestvedt, J., Gettelman, A., De León, R.R., Lim, L.L., Lund, M.T., Millar, R.J., Owen, B., Penner, J.E., Pitari, G., Prather, M.J., Sausen, R. and Wilcox, L.J.: The contribution of global aviation to anthropogenic climate forcing for 2000 to 2018, Atmospheric Environment, Volume 244, 117834, ISSN 1352-2310, https://doi.org/10.1016/j.atmosenv.2020.117834, 2021.

Lührs, B., Niklaß, M., Frömming, C., Grewe, V. and Gollnick, V.: Cost-benefit assessment of 2D- and 3D climate and weather optimized trajectories. In Proceedings of 16th AIAA Aviation Technology, Integration, and Operations Conference (ATIO). Washington D.C., USA, 2016.

Maruhashi, J., Grewe, V., Frömming, C., Jöckel, P., and Dedoussi, I. C.: Transport Patterns of Global Aviation NOx and their Short-term O3 Radiative Forcing – A Machine Learning Approach, Atmos. Chem. Phys. Discuss. [preprint], https://doi.org/10.5194/acp-2022-348, in review, 2022.

Petzold, A., and Karcher, B.: “Aerosols in the Atmosphere.” Atmospheric Physics Background, Methods, Trends, by U. Schumann, Springer, pp. 37–51, 2012.

Rao, P., Yin, F., Grewe, V., Yamashita, H., Jöckel, P., Matthes, S., Mertens, M., Frömming, C.: Case Study for Testing the Validity of NOx-Ozone Algorithmic Climate Change Functions for Optimising Flight Trajectories. Aerospace, 9, 231. https://doi.org/10.3390/aerospace9050231, 2022.

Righi, M., Hendricks, J., and Sausen, R.: The global impact of the transport sectors on atmospheric aerosol: simulations for year 2000 emissions, Atmos. Chem. Phys., 13, 9939–9970, https://doi.org/10.5194/acp-13-9939-2013, 2013.

Righi, M., Hendricks, J., and Sausen, R.: The global impact of the transport sectors on atmospheric aerosol in 2030 – Part 2: Aviation, Atmos. Chem. Phys., 16, 4481–4495, https://doi.org/10.5194/acp-16-4481-2016, 2016.

Simorgh, A., Soler, M., González-Arribas, D., Matthes, S., Grewe, V., Dietmüller, S., Baumann, S., Yamashita, H., Yin, F., Castino, F., Linke, F., Lührs, B., Meuser, M.M.: A Comprehensive Survey on Climate Optimal Aircraft Trajectory Planning. Aerospace, 9, 146. https://doi.org/10.3390/aerospace9030146, 2022.

Van Manen, J., and Grewe, V.: Algorithmic climate change functions for the use in eco-efficient flight planning. Transportation Research Part D: Transport and Environment, 67, 388-405, 2019.

Vehkamäki, H., Kulmala, M., Napari, I., Lehtinen, K. E. J., Timmreck, C., Noppel, M., and Laaksonen, A.: An improved parameterization for sulfuric acid-water nucleation rates for tropospheric and stratospheric conditions, J. Geophys. Res., 107, 4622–4631, doi:10.1029/2002JD002184, 2002.

Whitby, E. R., McMurry, P. H., Shankar, U., and Binkowski, F. S.: Modal aerosol dynamics modeling, Tech. Rep. EPA-68-01-7365, US Environmental Protection Agency, Office of Research and Development, Atmospheric Research and Exposure Assessment Laboratory, Research Triangle Park, NC, 1991.